Geophysical Journal International

Geophys. J. Int. (2022) **228,** 2122–2136
Advance Access publication 2021 October 23
GJI Seismology

https://doi.org/10.1093/gji/ggab432

The dispersive velocity of compressional waves in magmatic suspensions

Alexandre Carrara [1,2] Philippe Lesage,[2] Alain Burgisser,[2] Catherine Annen[2,3] and George W. Bergantz[1]

[1] *Department of Earth and Space Sciences, University of Washington, Box 35310, Seattle, WA 98195, USA. E-mail: carrara.alexandre.univ@gmail.com*
[2] *Université Grenoble Alpes, Université Savoie Mont Blanc, CNRS, IRD, UGE, ISTerre, 38000 Grenoble, France*
[3] *Institute of Geophysics, Academy of Sciences of the Czech Republic, Boční II/1401, 141 31 Prague 4, Czech Republic*

Accepted 2021 October 21. Received 2021 September 8; in original form 2021 March 30

SUMMARY

The geophysical detection of magma bodies and the estimation of the dimensions, physical properties and the volume fraction of each phase composing the magma is required to improve the forecasting of volcanic hazards and to understand transcrustal magmatism. We develop an analytical model to calculate *P* waves velocity in a three-phase magma consisting of crystals and gas bubbles suspended in a viscous melt. We apply our model to calculate the speed of sound as a function of the temperature in three magmas with different chemical compositions, representative of the diversity that is encountered in arc magmatism. The model employs the coupled phase theory that explicitly accounts for the exchanges of momentum and heat between the phases. We show that the speed of sound varies nonlinearly with the frequency of an acoustic perturbation between two theoretical bounds. The dispersion of the sound in a magma results from the exchange of heat between the melt and the dispersed phases that affects the magnitude of their thermal expansions. The lower bound of the sound speed occurs at low frequencies for which all the constituents can be considered in thermal equilibrium, whereas the upper bound occurs at high frequencies for which the exchange of heat between the phases may be neglected. The presence of gas in a magma produces a sharp decrease in the velocity of compressional waves and generates conditions in which the dispersion of the sound is significant at the frequencies usually considered in geophysics. Finally, we compare the estimates of our model with the ones from published relationships. Differences are largest at higher frequencies and are <10 per cent for typical magma.

Key words: Acoustic properties; Body waves; Physics of magma and magma bodies; Volcano seismology.

1 INTRODUCTION

Most upper crustal magma reservoirs are probably dominated by crystals. However, volumes dominated by the presence of fluids must exist if only episodically as evidenced by the crystal content of eruptive products (e.g. Pallister *et al*. 1996; Eichelberger & Izbekov 2000; Takahashi & Nakagawa 2013). The possible mechanisms leading to the presence of fluid-dominated magmatic volumes are the replenishment of crystal-rich magma reservoirs with crystal-poor magmas (e.g. Caricchi *et al*. 2014; Annen *et al*. 2015; Wiebe 2016; Carrara *et al*. 2020), and the extraction of melt or exsolved volatiles from crystal-rich reservoirs (e.g. Bachmann & Bergantz 2004; Huber *et al*. 2011; Parmigiani *et al*. 2016; Holness 2018; Bachmann & Huber 2019; Degruyter *et al*. 2019). The crystals and exsolved volatiles of a magma affect its rheology (e.g. Caricchi *et al*. 2007; Petford 2009; Mader *et al*. 2013) and can dramatically change eruptive styles (e.g. Karlstrom *et al*. 2012; Cassidy *et al*. 2018). When the solid volume fraction reaches a threshold, crystals start to touch each other, forming a semi-rigid skeleton inhibiting magma flow (Bergantz *et al*. 2017). In contrast, the volumes dominated by the presence of fluids represent the eruptible portions of the reservoir. Therefore, the detection of such volumes and the estimation of the volume fraction of each phase is of paramount importance to enhance our ability to predict the occurrence and style of eruptions and to best assess volcanic hazards.

Among geophysical methods, tomography of seismic wave velocities and attenuations has been widely employed to map magma reservoirs but has not clearly evidenced the presence of fluid-dominated bodies (Waite & Moran 2009; Paulatto *et al*. 2012; De Siena *et al*. 2014; Huang *et al*. 2015; Delph *et al*. 2017; Kiser *et al*. 2018; Hooft *et al*. 2019). Tomography images are computed with the first wave arrival at the stations, which corresponds to the fastest

travel from the source. The velocities of compressional waves (also called sound speed or *P*-wave velocity) are lower in fluid-rich magmas. As a result, the ray paths of the first arrivals may circumvent and undersample such volumes in the resulting images. The spatial averaging of the seismic properties resulting from tomography may also smooth the effects of the presence of small fluid bodies, which are then interpreted as partially molten rocks. Finally, seismic waves may be attenuated during their propagation across the magma reservoir. Hence, improving our knowledge of the acoustic properties of the materials constituting the magma reservoir can reduce the uncertainties in interpreting tomography images.

While models exist to compute the speed of sound and/or the associated attenuation coefficient in partially molten rocks (e.g. Mavko 1980; Hammond & Humphreys 2000; Takei 2002; Hier-Majumder 2008; Carcione *et al*. 2020) or in bubbly melts (e.g. Chouet 1996; Kumagai & Chouet 2000; Morrissey & Chouet 2001; Neuberg & O'Gorman 2002; Collier *et al*. 2006; Karlstrom & Dunham 2016), no model addresses the acoustic properties of magmas composed of crystals and gas bubbles suspended in the melt. Here, we aim at calculating the velocity of a compressional wave at the frequencies used in volcano seismology (∼0.001–1000 Hz) in a three-phase suspension composed of solids and gas bubbles suspended in a viscous liquid. Previous models for the acoustic properties of a suspension employed methods based on the effective medium theory (e.g. Kuster & Toksöz 1974; Berryman 1980) because they are applicable at any frequency, and account for the presence of an unlimited number of phases. However, this approach neglects the influence of the liquid phase viscosity, the relative motion (or relative velocity) between the constituents, the evolution of the temperature of the phases and the interaction between neighbouring solids grazing each other. Alternatively, methods using the coupled phase theory (e.g. Harker & Temple 1988; Atkinson & Kytömaa 1992; Margulies & Schwarz 1994; Kytömaa 1995; Evans & Attenborough 1997; Valier-Brasier *et al*. 2015) can capture all these effects for bi-phasic suspensions (e.g. solids in a liquid or bubbles in a liquid) but are restricted to the long-wavelength approximation (wavelength of the perturbation much larger than the size of the discrete phases). The coupled phase theory is suitable to compute the acoustic properties of magmas because the long-wavelength approximation is valid at the frequencies used in geophysics. To be extended to a three-phase magma, the method requires modifications to account for both viscous and thermal effects and the joint presence of crystals and gas bubbles.

Here, we adapt the coupled phase theory to the computation of the velocity of compressional waves travelling in magmas where the crystals are not touching each other and where the melt is the carrier phase. We first introduce the conservation equations controlling the propagation of an acoustic perturbation in a suspension and present the calculation of the speed of sound using the coupled phase theory. The resulting model allows us to compute both the velocity and the intrinsic attenuation coefficient of compressional waves. In this work, we focus on the speed of sound and we will address attenuation in a future communication. Results are first presented for a suspension representative of magmas to illustrate how its composition and the characteristics of the perturbation (frequency and propagation direction) affect the speed of sound. We then apply the model to magmas having different chemical compositions representative of arc magmatism to highlight the key features of the propagation of sound in magmas. Finally, we compare the results of our model with other relationships proposed or employed by authors to estimate compressional wave velocity in magmas.

2 METHOD

To present the model, we first introduce the physical model and assumptions about the initial conditions (Section 2.1). Then, we introduce the conservation equations describing the dynamics of the phases (Section 2.2). These equations are similar to those reported in the literature (e.g. Harker & Temple 1988; Atkinson & Kytömaa 1992; Evans & Attenborough 1997) and include a few modifications to account for the presence of three phases and the dynamic viscosity of the melt. The details of the derivation of these equations are presented in Supporting Information 1 (online). In Section 2.3, we present the relationships controlling the momentum transfer between the phases and within the liquid and solid phases. Section 2.4 details the relationships we used to account for the transfer of heat within the liquid phase and between the carrier and suspended phases. Section 2.5 describes briefly the calculation of the speed of sound using the coupled phase theory because we employed the same method as presented and employed by several authors to calculate the velocity of a compressional wave (e.g. Harker & Temple 1988; Atkinson & Kytömaa 1992; Evans & Attenborough 1997). We detail the calculation of the speed of sound in Supporting Information 2 (online). In Section 2.6, we derive the bounds of the speed of sound in magma using an alternative approach considering an isotropic compression of an isolated volume of magma. Finally, we present the initial composition of the magmas and how their changes in physical properties are computed as a function of temperature (Section 2.7).

2.1 Physical model

We consider an elementary volume of a suspension composed of solid particles and gas bubbles in a viscous liquid (Fig. 1). Both discrete phases are represented with monodisperse spheres. Initially, we consider all the constituents of the suspension to be static and in thermodynamic equilibrium. The thermodynamic properties of each phase (e.g. bulk modulus or specific heat capacity) are considered uniform within the elementary volume and constant with pressure and temperatures. The presence of mass transfer or chemical reactions between the phases is neglected.

A plane and monochromatic compressional wave propagates in a gravitational field in the direction x with an angle θ from the horizontal (Fig. 1). The geometry of the acoustic perturbation allows us to express the conservation equations describing the dynamics of each phase in one dimension aligned with the propagation direction x ($\partial y = \partial z = 0$). The wave has a small amplitude and a frequency in the range of the acoustic signals recorded in nature (0.001–1000 Hz) for which its wavelength is much larger than the diameters of the particles and bubbles. Therefore, the scattering of the acoustic wave resulting from resonance effects in the discrete solids and bubbles may be neglected (Atkinson & Kytömaa 1992).

2.2 Conservation equations

The propagation of an acoustic perturbation in the suspension is governed by the conservation equations of each phase. Neglecting the transfer of mass between the phases and chemical reactions, the conservation of mass of the liquid phase reads:

$$\partial_t \left(\phi_l \rho_l\right) + \partial_x \left(\phi_l \rho_l u\right) \; = \; 0, \tag{1}$$

where ρ_l is the density of the liquid phase, ϕ_l is the volume fraction of liquid in the suspension and u is the liquid velocity in the direction x ($u = u_x$, the velocities in the other directions are null because we

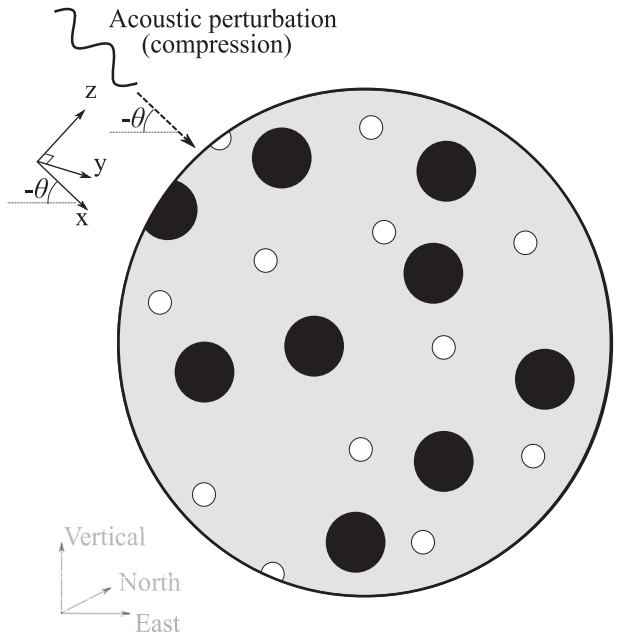

Figure 1. Schematic representation of a suspension of solid particles and gas bubbles in a viscous liquid. The scheme represents a cross-section of an elementary volume perpendicular to the north direction. The liquid phase is represented in grey. The black and white discs correspond to the solid particles and gas bubbles, respectively. The three grey axes (east, north and vertical) indicate the orientation with respect to the gravitational acceleration vector. The black orientation axes (x, y and z) indicate the coordinate system used to express the conservation equations, in which the direction x is aligned in the direction of the propagation of the wave. The sinusoid represents the plane acoustic perturbation propagating along the direction x with an angle θ (positive clockwise) from the east direction.

consider a plane wave and the suspension to be initially static). Similarly, for the solid and gas phases, mass conservations are:

$$\partial_t(\phi_s\rho_s) + \partial_x(\phi_s\rho_s v) = 0, \tag{2}$$

$$\partial_t(\phi_g\rho_g) + \partial_x(\phi_g\rho_g w) = 0, \tag{3}$$

where ρ_s is the density of the solids, ϕ_s is the volume fraction of solids, v is the velocity of the solids in the direction x, ρ_g is the gas density, ϕ_g is the volume fraction of gas and w is the velocity of the gas bubbles.

The rate of change of momentum of the liquid equals the sum of the applied force and may be expressed as (see Supporting Information 1, online):

$$\phi_l\rho_l(\partial_t(u) + u\partial_x(u)) + \phi_l\partial_x(P) + I_{ll} + I_{ls} + I_{lg} + \phi_l\rho_l g\sin\theta = 0, \tag{4}$$

where P is the pressure, I_{ll} is the rate of momentum exchange among the liquid, I_{ls} is the rate of momentum exchange between the liquid and solid phases, I_{lg} is the rate of momentum exchange between the liquid and gas phases and g is the gravitational acceleration. The exchange of momentum within the liquid, I_{ll}, is equal to the divergence of the viscous stress tensor and indicates the rate at which the viscous stress propagates in the liquid. The two other terms, I_{ls} and I_{lg}, express the exchanges of momentum between the carrier and discrete phases through the drag forces when they have relative velocities. The conservation of momentum in the solid phases is:

$$\phi_s\rho_s(\partial_t(v) + v\partial_x(v)) + \phi_s\partial_x(P) + I_{ss} - I_{ls} + \phi_s\rho_s g\sin\theta = 0, \tag{5}$$

where I_{ss} represents the transfer of momentum between close solids. Here, this term corresponds to the lubrication forces caused by the squeezing of the interstitial liquid located between two grazing particles (see the next section for details about this term). The momentum conservation in the gas phase reads:

$$\phi_g\rho_g(\partial_t(w) + w\partial_x(w)) + \phi_g\partial_x(P) - I_{lg} + \phi_g\rho_g g\sin\theta = 0. \tag{6}$$

The conservation of energy in the carrier liquid expressed as a function of the temperature reads:

$$\phi_l\rho_l C_{Pl}(\partial_t(T_l) + u\partial_x(T_l)) - \phi_l T_l\alpha_l(\partial_t(P) + u\partial_x(P)) + 2\phi_l\rho_l g u\sin\theta - \overline{\overline{\sigma_{xx}}}\partial_x(u) + H_{ll} + H_{ls} + H_{lg} = 0 \tag{7}$$

where T_l is the temperature of the liquid phase, C_{Pl} is the specific heat capacity at a constant pressure of the liquid, α_l is the coefficient of thermal expansion of the liquid, $\overline{\overline{\sigma}}$ is the liquid viscous stress tensor, H_{ll} is the rate of heat diffusion within the liquid phase by conduction, H_{ls} is the rate of heat exchange between the carrier liquid and discrete solids and H_{lg} is the rate of heat exchange between the liquid and gas bubbles. The two terms H_{ls} and H_{lg} are the total heat flux through the interfaces between the carrier and discrete phases. They depend on the temperature difference between constituents. Similarly, in the solid and gas phases, the conservation of energy is:

$$\phi_s\rho_s C_{Ps}(\partial_t(T_s) + v\partial_x(T_s)) - \phi_s T_s\alpha_s(\partial_t(P) + v\partial_x(P)) + 2\phi_s\rho_s g v\sin\theta - H_{ls} = 0, \tag{8}$$

$$\phi_g\rho_g C_{Pg}(\partial_t(T_g) + w\partial_x(T_g)) - \phi_g T_g\alpha_g(\partial_t(P) + w\partial_x(P)) + 2\phi_g\rho_g g w\sin\theta - H_{lg} = 0, \tag{9}$$

where T_s is the temperature of the solids, T_g is the temperature of the gas, C_{Ps} is the specific heat capacity at a constant pressure of the particles, C_{Pg} is the specific heat capacity of the gas, α_s is the coefficient of thermal expansion of the solid particles and α_g is the coefficient of thermal expansion of the gas.

The state equations link the variation of the density of the phases to the evolution of their temperatures and pressure:

$$d\rho_l - \frac{\rho_l}{K_l}dP + \alpha_l\rho_l\, dT_l = 0, \tag{10}$$

$$d\rho_s - \frac{\rho_s}{K_s}dP + \alpha_s\rho_s\, dT_s = 0, \tag{11}$$

$$d\rho_g - \frac{\rho_g}{K_g}dP + \alpha_g\rho_g\, dT_g = 0, \tag{12}$$

where K_l is the bulk modulus of the liquid phase (inverse of the coefficient of isothermal compressibility), K_s is the bulk modulus of the solids and K_g is the bulk modulus of the gas. The last conservation equation ensures that the sum of the volume fraction of all the phases is always equal to one. In differential form, it reads:

$$\partial_t(\phi_l) + \partial_t(\phi_s) + \partial_t(\phi_g) + u\partial_x(\phi_l) + v\partial_x(\phi_s) + w\partial_x(\phi_g) = 0. \tag{13}$$

2.3 Interphase exchanges of momentum

The exchange of momentum within the liquid phase, I_{ll}, is equal to the divergence of the viscous stress tensor, $\overline{\overline{\sigma}}$, which depends on the dynamic shear viscosity, η and volume viscosity, λ, of the liquid ($I_{ll} = \phi\nabla\cdot[\eta\overline{\overline{\dot{\epsilon}}} + \lambda tr(\overline{\overline{\dot{\epsilon}}})\overline{\overline{I}}]$, where $\overline{\overline{\dot{\epsilon}}}$ is the strain rate tensor and $\overline{\overline{I}}$ is the unit tensor). For a magmatic melt in relaxed conditions (low-frequency perturbations), Dingwell & Webb (1989) showed that $\lambda = \eta/3$. Since the velocity of the liquid in the directions y and z are

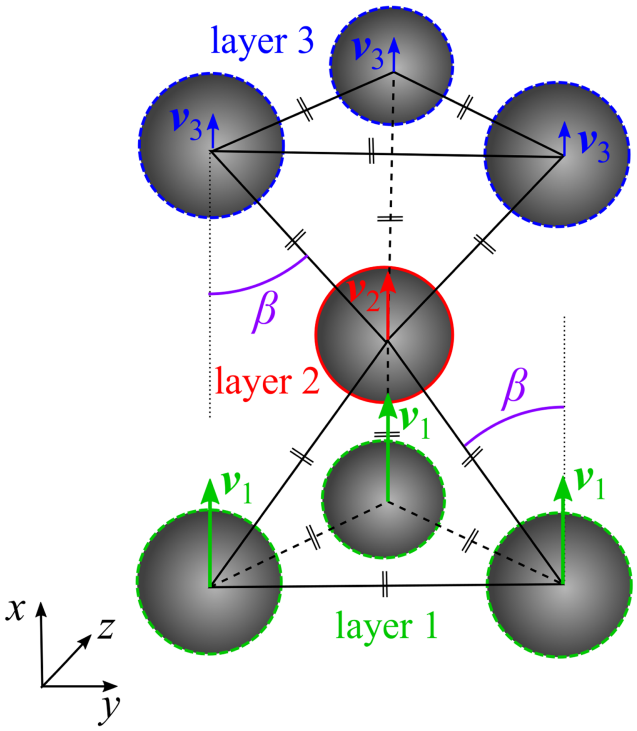

Figure 2. Conceptual configuration of the crystals used to derive the rate of momentum exchange between the solids. The scheme represents one target particles located in the layer 2 and its six closest neighbours located in layers 1 and 3. The colour of the boundary of each particle depends on the layer in which it is located (green for layer 1, red for layer 2 and blue for layer 3). Each arrow indicates the velocity vector of the corresponding particles. The grazing angle β is represented in purple.

null, the rate of momentum exchange in the liquid can be calculated as:

$$I_{ll} = \frac{7}{3}\,\phi_l \eta \partial_x^2 (u)\,. \tag{14}$$

While contacts are neglected, crystals can exchange momentum through lubrication forces (Marzougui *et al*. 2015; Bergantz *et al*. 2017; Carrara *et al*. 2019). Lubrication refers to the hydrodynamic forces resulting from the resistance of the liquid located in the gap between two neighbouring particles to their relative motions. These forces influence the duration of the initiation and closure of motion of the solid phase (Carrara *et al*. 2019)**.** The propagation of a wave in a suspension can be viewed as a 'cyclical transient' in which the relative motions between neighboring solids are repetitively initiated and dissipated. To derive an expression of the rate of momentum exchange between the solids, I_{ss}, we consider a suspension where spherical particles are regularly organized forming a hexagonal close-packed lattice (Fig. 2). In this configuration, the distances between the particles are identical and minimized such that the influence of lubrication is maximized. The solid lattice is oriented along the direction of propagation of the wave (x) such that it can be represented as three layers of particles orthogonal to the direction x (Fig. 2). The total lubrication force between two neighboring particles (here labelled as i and k) including both normal and tangential components can be expressed as (Marzougui *et al*. 2015; Carrara *et al*. 2019):

$$F_{\text{lub}}\ (k,i) = \frac{3\eta A}{\rho_s {d_s}^2}\ (v_k - v_i)\,, \tag{15}$$

where A is a geometrical parameter indicating the relative importance between normal and tangential lubrication forces that depends on the distance between the surface of the particles and on the grazing angle β (Carrara *et al*. 2019):

$$A = \frac{3\cos\beta}{2j} - \ln(j)\sin\beta, \tag{16}$$

where j is the ratio between the distance separating the surface of the neighbouring particles and their radius. Both the incidence angle and distance between the surface of the particles can be deduced from geometrical arguments since the solid lattice is regular. For a compressional wave $\beta = (2/3)^{1/2}$ and j is related to the volume fraction of solids by (Atkinson & Kytömaa 1992):

$$j\ =\ 1 - \left(\frac{\phi_s}{\phi_{s\,\max}}\right)^{\frac{1}{3}}, \tag{17}$$

where $\phi_{s\,\max}$ is the maximum volume fraction at which the solids start to touch each other. For a hexagonal close-packed lattice, $\phi_{s\,\max} = 0.64$. Summing all the lubrication interactions experienced by the particle located on the second layer in Fig. 2 gives:

$${F_{\text{lub}}}^{\text{tot}}\ (2) = \frac{9\eta A}{\rho_s {d_s}^2}\ (v_1 + v_3 - 2v_2)\,, \tag{18}$$

where v_1, v_2 and v_3 are the velocity of the particles in the layers 1, 2 and 3, respectively. The sum of the solid velocities on the right-hand side of eq. (18) may be approximated with the second-order derivative in space of the solid velocity:

$$\frac{\partial^2 v_x}{\partial x^2} \simeq \frac{(v_1 + v_3 - 2v_2)}{{\Delta_x}^2}, \tag{19}$$

where Δ_x is the distance in the direction x separating two successive layers of solids in Fig. 2, which can be calculated as:

$$\Delta_x = \sqrt{\frac{2}{3}}\, d_s \left(\frac{j}{2} + 1\right). \tag{20}$$

Inserting eqs (19) and (20) into eq. (18) gives the following expression for the exchange of momentum between the solids:

$$I_{ss} = F_{\text{lub}}\ \simeq \frac{6\eta A\left(\frac{j}{2}+1\right)^2}{\rho_s}\frac{\partial^2 v}{\partial x^2}. \tag{21}$$

The liquid exchanges momentum with the other phases (particles and bubbles) because of their relative motions. The transfers of momentum between the carrier and discrete phases include both steady (drag) and unsteady (added mass and Basset forces) contributions. Because of the high viscosity of magmatic melts, the frequency range considered here is well below those at which unsteady forces become significant compared to the steady contribution (Gumerov *et al*. 1988; Atkinson & Kytömaa 1992). Therefore, the rate of momentum exchange between the liquid and solid phases can be reduced to the steady term (Gidaspow 1994):

$$I_{ls} = \beta_{ls}\ (u - v)\,, \tag{22}$$

and the rate of momentum exchange between liquid and bubbles is:

$$I_{lg} = \beta_{lg}\ (u - w)\,, \tag{23}$$

where β_{ls} is the coefficient of momentum exchange between the liquid and solids and β_{lg} is the coefficient of momentum exchange between the liquid and gas phases. To compute these two coefficients, several empirical correlations exist in the literature (e.g. Ergun 1952; Wen & Yu 1966; Syamlal *et al*. 1993; Gidaspow 1994;

Benyahia *et al*. 2006). Here, we combine a Stokes drag law for high porosity (high liquid volume fraction) and an Ergun relationship at lower liquid volume fraction. Because of the high viscosity of the liquid phase, the Ergun drag law may be reduced to the Carman–Kozeny relationship because the inertial term becomes negligible:

$$\beta_{ls} = \begin{cases} \dfrac{18\eta\phi_s}{{d_s}^2} & if\,\phi_l > \dfrac{25}{28} \\ \dfrac{150{\phi_s}^2\eta}{\phi_l{d_s}^2} & if\,\phi_l \leq \frac{25}{28} \end{cases}, \tag{24}$$

$$\beta_{lg} = \begin{cases} \dfrac{18\eta\phi_g}{{d_g}^2} & if\,\phi_l > \dfrac{25}{28} \\ \dfrac{150{\phi_g}^2\eta}{\phi_l{d_g}^2} & if\,\phi_l \leq \frac{25}{28} \end{cases}, \tag{25}$$

where d_s is the diameter of the solid particles and d_g is the diameter of the gas bubbles. The drag laws we used here are similar to the one proposed by Gidaspow (1994), but uses the Stokes drag instead of the Wen–Yu drag correlation at high porosity such that the drag forces are linearly dependent on the relative velocities between the phases, which is suitable for the coupled phase theory.

2.4 Interphase exchanges of heat

The amount of heat transferred within the carrier liquid by conduction is calculated using Fourier's law:

$$H_{ll} = \phi_l\, k_l \partial_x^2\,(T_l)\,, \tag{26}$$

where k_l is the heat conductivity of the liquid.

The rate of heat exchange between the carrier and discrete phases are expressed by:

$$H_{ls} = \gamma_{ls}\ (T_l - T_s)\,, \tag{27}$$

and,

$$H_{lg} = \gamma_{lg}\ \left(T_l - T_g\right), \tag{28}$$

where γ_{ls} is the coefficient of heat transfer between the fluid and solids and γ_{lg} is the coefficient of heat exchange between the fluid and gas. In the absence of mass transfer between the phases, the coefficients of heat transfer can be estimated as (Syamlal *et al*. 1993):

$$\gamma_{ls} = \frac{6k_l\phi_s Nu}{{d_s}^2}\,, \tag{29}$$

and,

$$\gamma_{lg} = \frac{6k_l\phi_g Nu}{{d_g}^2}\,, \tag{30}$$

where Nu is the Nusselt number. To estimate Nu, we used the empirical correlation proposed by Gunn (1978), which depends on both the porosity and relative velocity between the phases. Since in our case the relative velocities are very small because of the small amplitude of the perturbation and the viscosity of the liquid, Nu may be expressed as a function of ϕ_l only:

$$Nu\ = \left(7 - 10\phi_l + 5{\phi_l}^2\right)\,. \tag{31}$$

2.5 Coupled phase model

To compute the speed of sound from eqs (1) to (13), we employed the coupled phase theory (e.g. Harker & Temple 1988; Atkinson & Kytömaa 1992; Evans & Attenborough 1997; Valier-Brasier *et al*. 2015; see Supporting Information 2, online, for details about the method and equations), which consists in imposing a small and monochromatic perturbation to all the variables that oscillate during the propagation of the acoustic perturbation (ρ_l, ρ_s, ρ_g, u, v, w, T_l, T_s, T_g, ϕ_l, ϕ_s, ϕ_g, P) by using wave-like solutions (here for the density of the liquid phase):

$$\rho_l = {\rho_l}^0\ + \overline{\rho_l} e^{i(kx-\omega t)}, \tag{32}$$

where ${\rho_l}^0$ is the static fluid density, $\overline{\rho_l}$ is the amplitude of the perturbation of the fluid density at the source and $i^2 = -1$. Note that since all phases are static and in thermal equilibrium before the perturbation, $u_0 = v_0 = w_0 = 0$ and ${T_l}^0 = {T_s}^0 = {T_g}^0 = T^0$. The exponential term in eq. (32) expresses the spatial and temporal variations of the liquid density and depends on ω, the angular frequency ($\omega = 2\pi f$, f is the frequency of the perturbation), and k the complex wavenumber defined as:

$$k\ = \frac{\omega}{c}\ + i\alpha, \tag{33}$$

where c is the speed of sound and α is the associated intrinsic attenuation coefficient. After the introduction of the oscillating variables and linearization (the products of two small oscillations are neglected), the set of equations can be expressed as a matrix equation (see Supporting Information 1 for details about the matrix equation):

$$M\left[\overline{\rho_l}, \overline{\rho_s}, \overline{\rho_g}, \overline{\phi_l}, \overline{\phi_s}, \overline{\phi_g}, \overline{T_l}, \overline{T_s}, \overline{T_g}, \bar{u}, \bar{v}, \bar{w}, P\right]^T\ =\ 0, \tag{34}$$

where $\boldsymbol{M}$ is a coefficients matrix containing k as unique unknown. To ensure the equality in eq. (34), the non-trivial solution (a perturbation exists) imposes that $\boldsymbol{M}$ is singular and thus:

$$det\,(M)\ =\ 0. \tag{35}$$

The speed of sound and associated attenuation coefficient at a given frequency can be found from the wavenumber, k, that is physically meaningful and that satisfies eq. (35).

2.6 Bounds of the sound speed in magmas

The speed of sound in a suspension depends on the variation of its density and volume during an adiabatic compression or dilatation (Temkin 1998). Consider an elementary volume, V, containing a constant mass of solids and gas bubbles suspended in a viscous liquid. By neglecting the relative motions between the phases, the suspension can be approximated as a homogeneous material having a bulk density, $\rho*$, defined as (Brennen 2005):

$$\rho*\ = \phi_l\ \rho_l + \phi_s\rho_s + \phi_g\rho_g. \tag{36}$$

The total net change of the elementary volume, dV, can be written as the sum of the net changes of the volume of the three phases:

$$dV\ = dV_l\ + dV_s + dV_g, \tag{37}$$

where dV_l is the net change of the volume of liquid, dV_s is the net change of the volume of solid and dV_g is the net change of the volume of gas. Neglecting phase changes, eq. (37) may be expressed as:

$$\frac{d\rho*}{\rho*} = \frac{\phi_l}{\rho_l}\,d\rho_l + \frac{\phi_s}{\rho_s}d\rho_s + \frac{\phi_g}{\rho_g}d\rho_g, \tag{38}$$

where $d\rho*$ is the net change in the bulk density of the suspension, $d\rho_l$ is the net change of the liquid density, $d\rho_s$ is the net change of the density of the solids and $d\rho_g$ is the net change of the density of the gas bubbles. The evolution of the density of each phase depends on the change in pressure (here we consider that the pressure is the

same in all the phases) and in its temperature as (here for a phase i):

$$d\,\rho_i = \left(\frac{\partial \rho_i}{\partial P}\right)_T dP + \left(\frac{\partial \rho_i}{\partial T_i}\right)_P dT_i, \tag{39}$$

where $(\partial \rho_i/\partial P)_T$ is the variation of the density of a constituent with the pressure at a constant temperature and $(\partial \rho_i/\partial T_i)_P$ is the derivative of its density with respect to its temperature at a constant pressure. Introducing eqs (39) into (38) yields:

$$\frac{d\rho*}{\rho*} = \frac{1}{K*}\,dP + \frac{\phi_l}{\rho_l}\left(\frac{\partial \rho_l}{\partial T_l}\right)_P dT_l + \frac{\phi_s}{\rho_s}\left(\frac{\partial \rho_s}{\partial T_s}\right)_P dT_s + \frac{\phi_g}{\rho_g}\left(\frac{\partial \rho_g}{\partial T_g}\right)_P dT_g, \tag{40}$$

where $K*$ is the bulk modulus characterizing the suspension and defined as:

$$\frac{1}{K_*} = \frac{\phi_l}{K_l} + \frac{\phi_s}{K_s} + \frac{\phi_g}{K_g}, \tag{41}$$

with $K_l/\rho_l = (\partial P/\partial \rho_l)_T$, $K_s/\rho_s = (\partial P/\partial \rho_s)_T$ and $K_g/\rho_g = (\partial P/\partial \rho_g)_T$. When the net changes in temperature of the phases are neglected, the isothermal speed of sound is:

$$c^{-2} = \frac{d\rho*}{dP} = \frac{\rho*}{K*}. \tag{42}$$

When considering temperature variations, the speed of sound depends on the evolution of the bulk density of the suspension with pressure at constant entropy (Temkin 2000)**.** The net change of entropy, dS, in each phase may be expressed as a function of the net change in its temperature and pressure (here for a phase i):

$$T_i\,dS_i = \left(\frac{\partial S_i}{\partial T_i}\right)_P dT_i + \left(\frac{\partial S_i}{\partial P}\right)_T dP. \tag{43}$$

Considering an isentropic transformation, eq. (43) can be expressed as:

$$\left(\frac{\partial T_i}{\partial P}\right)_S = -\left(\frac{\partial T_i}{\partial S_i}\right)_P \left(\frac{\partial S_i}{\partial P}\right)_T. \tag{44}$$

Because the magma constituents have different thermodynamic properties, the net changes in temperature of the phases for the same net change in pressure are not equal. Two end-member scenarios may be considered as a function of the perturbation frequency and characteristic times for the phases to reach thermal equilibrium, τ. When $f \gg \tau^{-1}$, the heat exchanges between the phases may be neglected such that $dT_l \neq dT_s \neq dT_g$. Inserting eq. (44) into eq. (40) and considering the relationships $dTi = (\partial T_i/\partial P)_S\,dP$, $(\partial T_i/\partial S_i)_P = T_i/C_{Pi}$, $(\partial S_i/\partial P)_T = -\alpha_i/\rho_i$ and $(\partial \rho_i/\partial T)_P = -\alpha_i\,\rho_i$, the speed of sound at thermal disequilibrium reads:

$$c^{-2} = \frac{d\rho*}{dP} = \rho*\left(\frac{1}{K*} - \frac{\phi_l \alpha_l^2 T^0}{C_{Pl}\rho_f} - \frac{\phi_s \alpha_s^2 T^0}{C_{Ps}\rho_s} - \frac{\phi_g \alpha_g^2 T^0}{C_{Pg}\rho_g}\right). \tag{45}$$

When $f \ll \tau^{-1}$, the rates of heat exchanges between the phases are efficient such that the phases may be considered in thermal equilibrium during the propagation of the perturbation. In adiabatic conditions, the total change of temperature in the suspension at equilibrium, $dT*$, may be calculated as:

$$dT* = \frac{\phi_l \rho_l C_{Pl} dT_l + \phi_s \rho_s C_{Ps} dT_s + \phi_g \rho_g C_{Pg} dT_g}{\phi_l \rho_l C_{Pl} + \phi_s \rho_s C_{Ps} + \phi_g \rho_g C_{Pg}}. \tag{46}$$

Setting $dT_l = dT_s = dT_g = dT*$ in eq. (40) and inserting eqs (44) and (46) give the following relationship for the speed of sound at thermal equilibrium:

$$c^{-2} = \frac{d\rho*}{dP} = \frac{\rho*}{K*} - \frac{\alpha*^2 T^0}{C_{P*}}, \tag{47}$$

where $\alpha*$ is the bulk coefficient of thermal expansion defined as:

$$\alpha* = \phi_l\,\alpha_l + \phi_s \alpha_s + \phi_g \alpha_g, \tag{48}$$

and C_{P*} is the specific bulk heat capacity at constant pressure calculated as a mass average:

$$C_{P*} = \frac{\phi_l \rho_l C_{Pl} + \phi_s \rho_s C_{Ps} + \phi_g \rho_g C_{Pg}}{\rho_*}. \tag{49}$$

The characteristic time at which the transition between the two regimes occurs depends on the rate at which the heat is exchanged between the phases. Two characteristic times may be calculated since both the gas and solids are suspended in the liquid. To estimate these critical frequencies, we start by considering a static suspension of gas bubbles in a liquid. The evolution of the difference in temperature between the two phases resulting only from the heat exchanged between them may be approximated as:

$$\partial_t \left(T_l - T_g\right) + \tau_g^{-1}\left(T_l - T_g\right) = 0. \tag{50}$$

where τ_g is the characteristic time to equilibrate the temperature of the liquid and the gas phases given by:

$$\tau_g^{-1} = \gamma_{lg}\left(\frac{1}{\phi_l \rho_l C_{Pl}} + \frac{1}{\phi_g \rho_g C_{Pg}}\right). \tag{51}$$

Similarly, the characteristic time to equilibrate the temperature of the phases in a suspension of solids in a liquid, τ_s, is:

$$\tau_s^{-1} = \gamma_{ls}\left(\frac{1}{\phi_l \rho_l C_{Pf}} + \frac{1}{\phi_s \rho_s C_{Ps}}\right). \tag{52}$$

2.7 Magmas under consideration

We considered three different magmas representative of compositions that may be encountered in arc magmatism (basalt, andesite and dacite) and simulated their adiabatic cooling and crystallization using the software MELTS (Ghiorso 2004) at a pressure of 150 MPa and fixing the oxygen fugacity along the Ni–NiO oxygen buffer for the andesite and dacite, and along the quartz–fayalite–magnetite buffer for the basalt. The initial compositions were taken from Dufek & Bachmann (2010) and Martel *et al*. (1999) (see Table 1). We set the initial amount of dissolved water in the magmas to ∼3.5 wt. per cent to ensure that water vapour starts exsolving once the mass fraction in liquid is ∼70 wt. per cent (Duan 2014). We used the thermodynamic properties of each phase computed during the cooling simulations to estimate the speed of sound in the magmas as a function of their temperature. All the simulations were stopped when the crystallinity of the magmas reached the maximum packing fraction ($\phi_l = 0.36$).

3 RESULTS

3.1 The speed of sound in three phases suspensions

To illustrate how the material properties and characteristics of the perturbation affect the speed of sound in magmas, we define reference conditions relevant to magmas (Table 2) and vary selected parameters independently from each other. Fig. 3(a) displays the evolution of the velocity of a compressional wave as a function of the volume fraction in liquid, solids and gas bubbles when $f = 0.01$ Hz.

Table 1. Initial chemical composition, pressure and temperature of the magmas.

Composition wt. per cent	Basalt	Andesite	Dacite
SiO_2	48.108	59.736	66.013
TiO_2	0.970	0.469	0.440
Al_2O_3	16.883	17.341	15.263
Fe_2O_3	1.755	1.277	0.663
FeO	8.279	4.765	2.031
MnO	0.174	0.176	0.069
MgO	5.925	2.239	0.908
CaO	10.396	6.100	2.910
Na_2O	2.657	3.451	3.691
K_2O	1.193	1.026	4.004
P_2O_5	0.214	0.000	0.186
H_2O	3.447	3.4213	3.435
T start (°C)	1100	1050	950
T stop (°C)	960	700	715
P (MPa)	150	150	150
fO_2 buffer	QFM	Ni–NiO	Ni–NiO
Source	Dufek & Bachmann (2010)	Martel *et al.* (1999)	Dufek & Bachmann (2010)

Table 2. Reference physical properties used to explore the influence of the composition of the suspension and characteristics of the perturbation on the speed of sound. They correspond to an approximate total pressure of 150 MPa

Variable	Reference value
T	1000 °C
ρ_l^0	2500 kg m^{-3}
ρ_s^0	3000 kg m^{-3}
ρ_g^0	350 kg m^{-3}
K_l	15 GPa
K_s	50 GPa
K_g	150 MPa
η	1000 Pa s
C_{Pl}	1300 J kg^{-1} K^{-1}
C_{Ps}	1200 J kg^{-1} K^{-1}
C_{Pg}	3750 J kg^{-1} K^{-1}
α_l	10^{-4} K^{-1}
α_s	10^{-6} K^{-1}
α_g	10^{-3} K^{-1}
k_l	1 W m^{-1} K^{-1}
d_s	5 mm
d_g	0.5 mm
g	−9.81 m s^{-2}
θ	0°

It shows that the speed of sound decreases rapidly once a small volume fraction of volatiles is exsolved. When $\phi_g > 0.05$, the solid volume fraction has a negligible influence on the compressional wave velocity compared to that in the presence of gas.

Fig. 3(b) displays the speed of sound in the same suspension as in Fig. 3(a) when $f = 100$ Hz. Results show the same dependence of the wave velocity on ϕ_g. The amplitude of the decrease of the speed of sound when increasing the volume fraction of gas is, however, slightly lower as illustrated by the shift of the position of the isocontour of $c = 500$ m s^{-1}. The frequency of the perturbation changes both the minimum ($c \approx 457$ m s^{-1} when $f = 0.01$ Hz and $c \approx 482$ m s^{-1} when $f = 100$ Hz) and maximum ($c \approx 3117$ m s^{-1} when $f = 0.01$ Hz and $c \approx 3150$ m s^{-1} when $f = 100$ Hz) velocities computed by the model. On the contrary, when $\phi_l = 1$ the speed of sound is the same at the two frequencies (2582 m s^{-1}).

To further investigate the influence of the perturbation frequency on sound speed in a magma, we set the volume fractions of its constituents to $\phi_l = 0.65$, $\phi_s = 0.3$ and $\phi_g = 0.05$ and calculate the dispersion curve of the acoustic waves (Fig. 4). Results show that the speed of sound increases nonlinearly with the frequency and that three plateaus can be identified. The lowest plateau at $c \approx 1020$ m s^{-1} occurs when $f < 0.01$ Hz. The second velocity plateau at $c \approx 1025$ m s^{-1} occurs when 0.1 Hz $< f <$ 1 Hz, whereas the third and fastest one at $c \approx 1090$ m s^{-1} is reached when $f > 100$ Hz. As illustrated in Fig. 4, the uppermost plateau occurs when $f \gg \max(\tau_s^{-1}, \tau_g^{-1})$ and corresponds to the thermal disequilibrium bound of the speed of sound predicted by eq. (45). The lowest plateau is found when $f \ll \min(\tau_s^{-1}, \tau_g^{-1})$ and corresponds to thermal equilibrium bound of the speed of sound given by eq. (47). The isothermal bound (eq. 42) underestimate the speed of sound at all frequencies.

Fig. 5 displays the evolution of the wave velocity as a function of the propagation angle, θ, and frequency of the perturbation. When $f \geq 0.1$ Hz, the velocity of the wave is lower when the wave propagates upward than when it propagates downward. When $f < 0.1$ Hz, the speed of sound show a complex dependence on the propagation angle. The maximum velocity is computed when $\theta = \pi/2$, whereas the minimum sound speed occurs when the wave propagates downward with a propagation angle of ∼30° from the horizontal. The propagation angle influences sound speed because of the terms involving the gravitational acceleration in eqs (4)–(9). In momentum conservation, these terms express the contribution of the change in the density of the phases to the gravitational force. In the energy conservations, the term involving the gravitational acceleration expresses the rate at which the potential energy changes as a function of the velocity of the phase along the vertical direction. However, the variations in wave velocities as a function of the propagation angle (<1 per cent) are negligible compared to the influences of the volume fraction of the constituents (Fig. 3) and frequency of the perturbation (Fig. 4).

Fig. 6(a) displays the difference between the velocity of a compressional wave computed when lubrication is accounted for and when it is neglected as functions of the ratio of the solid volume fraction over the maximum packing fraction, $\phi_s/\phi_{s\,\max}$, and the perturbation frequency. The difference increases with the ratio $\phi_s/\phi_{s\,\max}$ and with wave frequency. When $f < 10^5$ Hz, the influence of lubrication forces on the velocity of a *P* wave is negligible. Lubrication forces have some influence of sound speed in a magma only at high frequency ($f > 10^6$ Hz).

3.2 Application to magmas

Figs 7(a)–(e) displays the evolution of the phase assemblages and thermodynamic properties of the three magmas computed by the cooling simulations and averaged over the phases with eqs (35), (42), (45) and (47) (see Supporting Information 3, online, for details on the thermodynamic properties of the constituents). The thermodynamic properties show sharp changes once the water vapour is exsolved. The bulk moduli of the magmas, in particular, drop by almost one order of magnitude once a small fraction of water is exsolved (Fig. 7d), resulting in a sharp decrease of the sound speed (Fig. 7f). In the absence of gas, the influence of the frequency of the perturbation is weak enough for the lower (eq. 47) and upper (eq. 45) bounds of the *P*-wave velocity to be almost equal. On the contrary, the two bounds show significant differences when a gas

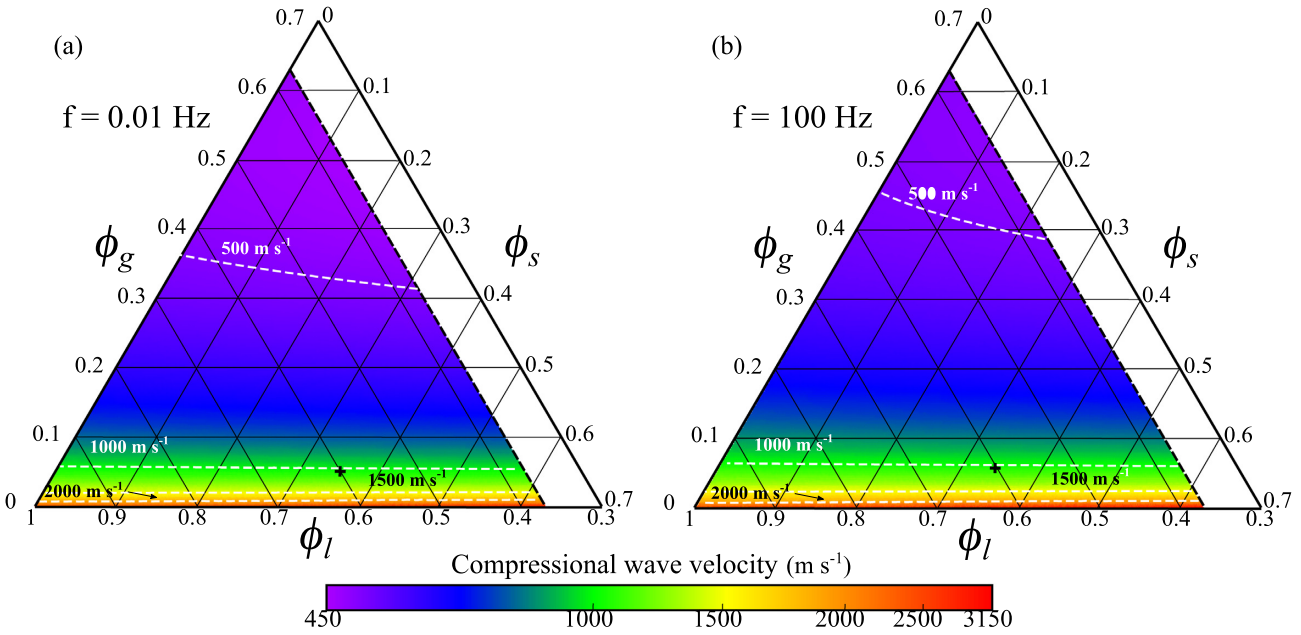

Figure 3. Speed of sound as a function of the volume fraction in liquid, solids and gas when (a) $f = 0.01$ Hz and (b) $f = 100$ Hz. The background colour depends on the speed of compressional waves. The white dashed curves indicate isocontours of the sound speed. The black dashed line indicates the theoretical limit of the validity of the model at $\phi_l = 0.36$. The material properties of the constituents and the incidence angle are indicated in Table 2. The black cross indicates the volume fractions used to compute the dispersion curve in Fig. 4.

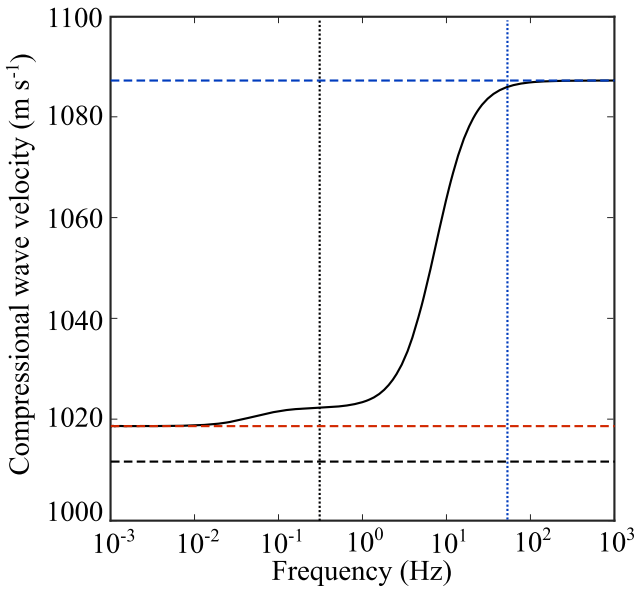

Figure 4. Dispersion curve of a magmatic suspension. The volume fraction of the constituents are $\phi_l = 0.6$, $\phi_s = 0.35$ and $\phi_g = 0.05$. The solid black curve indicates the results obtained with the coupled phase theory (eq. 35). The black, red and blue dashed lines indicate the isothermal speed of sound (eq. 42), the isentropic speed of sound at thermal equilibrium (eq. 47), and the isentropic speed of sound out of thermal equilibrium (eq. 45), respectively. The black and blue vertical dotted lines indicate the critical frequencies above which the solid and gas bubbles are not in thermal equilibrium with the surrounding liquid, respectively (eqs 51 and 52). The material properties of the constituents and the incidence angle are indicated in Table 2.

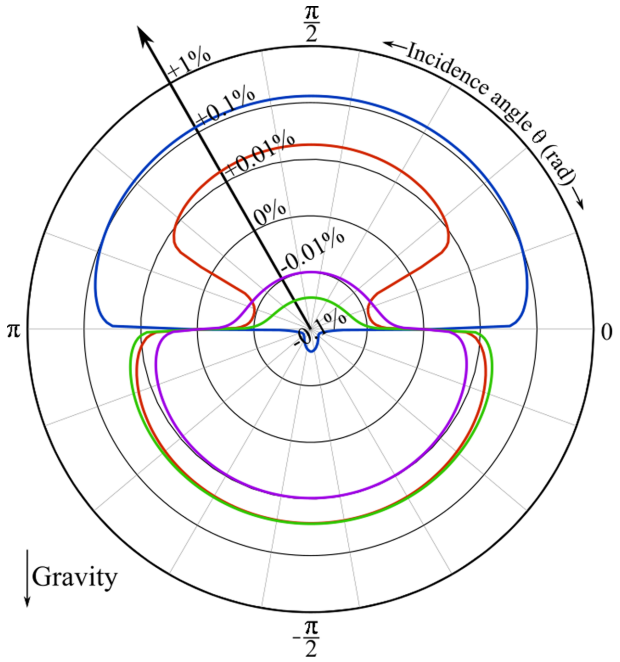

Figure 5. Evolution of the compression wave velocity as a function of the incidence angle and frequency of the perturbation. The radial axis indicates the difference in per cent between the velocity of the compressional wave at θ and $\theta = 0$. The blue, red, green and purple curves correspond to frequencies of 0.01, 0.1, 1 and 10 Hz, respectively. The volume fraction of the constituents are $\phi_l = 0.65$, $\phi_s = 0.3$ and $\phi_g = 0.05$. The material properties of the constituents are indicated in Table 2.

phase is present (Fig. 7f). The amplitude of the difference between the two bounds increases with the volume fraction of gas and decreases with temperature. In the final phases assemblages, the gas volume fractions are $\phi_g \approx 0.15$ in the basalt (Fig. 7a), $\phi_g \approx 0.1$ in the andesite (Fig. 7b) and $\phi_g \approx 0.05$ in the dacite (Fig. 7c). These values translate into amplitude differences between the upper and lower bounds of ~150 m s^{-1} in the basalt, ~200 m s^{-1} in the andesite and ~250 m s^{-1} in the dacite (Fig. 7f).

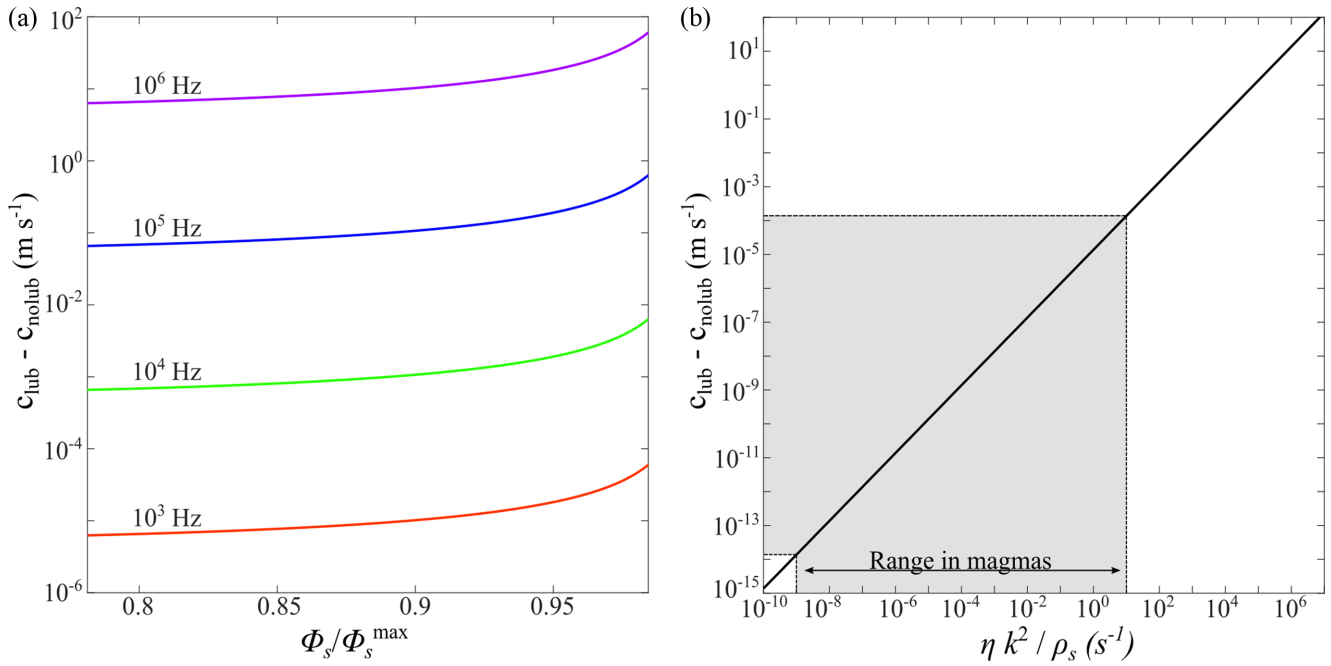

Figure 6. Influence of the lubrication forces on the speed of sound in a suspension of solid particles in a viscous fluid. (a) Difference between the speed of sound computed with eq. (35) considering and neglecting lubrication forces. The physical properties of the liquid and solids are the ones indicated in Table 2. (b) Evolution of the difference between the speed of sound computed with eq. (35) considering (c_{lub}) and neglecting (c_{nolub}) lubrication forces as a function of $\eta k^2/\rho_s$. The shaded area indicates the area covered by magmas.

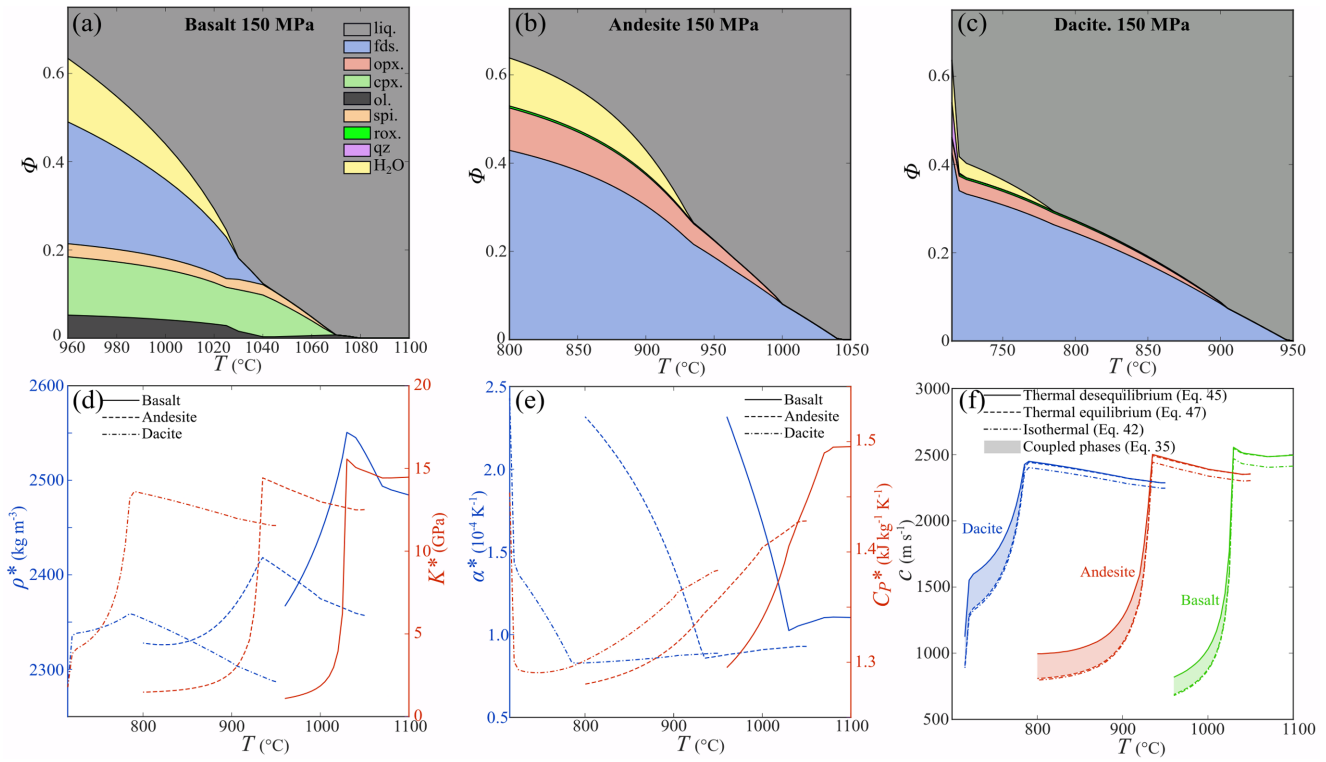

Figure 7. Evolution of the phase assemblage, thermodynamic properties, and speed of sound of the magmas during the cooling simulations. (a)–(c) are the phases assemblage computed during the simulation of the cooling of the (a) basalt, (b) andesite and (c) dacite. (d) Evolution of the bulk densities and bulk moduli of the magmas. (e) Evolution of the bulk coefficient of thermal expansion and bulk heat capacity at constant pressure as a function of temperature. (f) Evolution of the speed of sound in the magmas. The solid, dashed and dashed–dotted curves indicate the thermal disequilibrium (high frequency), thermal equilibrium (low frequency) and isothermal bounds, respectively. The shaded areas correspond to the range of velocity that may be computed with eq. (35) at different frequencies.

Table 3. List of the thermodynamical properties, or expressions employed to estimate them, used to compare the different models in Fig. 8. The surface tension at the interfaces between the bubbles and liquid is neglected. The thermodynamic properties and relationships are taken from Kieffer (1977).

Parameters	Expression or value
${\rho_l}^0$	1000 kg m^{-3}
${\rho_g}^0$	$\rho_g^0 = (\frac{P}{G_{\rm air}})^{\frac{1}{\gamma}}$
${\rho_g}^{\rm ref}$	690 kg m^{-3}
$G_{\rm air}$	$G_{\rm air} = \frac{TR}{M_g {\rho_g}^{{\rm ref}\,\gamma-1}}$
T	20 °C
P	500 bars
γ	1.4
d_g	0.5 mm
η	10 Pa·s
M_g	29.98×10^{-3} kg mol^{-1}
C_{Pl}	1300 J kg^{-1} K^{-1}
C_{Pg}	$C_{Pg} = \frac{R}{M_g}(1-\frac{1}{\gamma})$
K_f	1 GPa
K_g	$K_g = P$
α_l	1×10^{-4} K^{-1}
α_g	$\alpha_g = 1/T$

The dispersion of sound is particularly important in bubbly magmas (Fig. 3 and Fig. 7F). In general, $\alpha_g/(\rho_g\, C_{pg}) \gg \alpha_l/(\rho_l\, C_{pl})$. As a result, for the same net change in pressure, $|dT_l| < |dT*| < |dT_g|$ (eq. 44). Since $\alpha_g \gg \alpha_f$, the net thermal expansion of the gas bubbles increases significantly out of thermal equilibrium, which in turn amplifies the resistance of the bulk material to compression and decompression and increases the speed of sound (Temkin 2000). This effect results in the two increases of the speed of sound with frequency observed in Fig. 4. The first increase occurs when the solids become out of thermal equilibrium with the liquid. This velocity jump may be ignored in crystal-bearing magmas (Fig. 7f) because the coefficients of thermal expansion of the melt and crystals are small (see Supporting Information 3, online).

4 DISCUSSION

4.1 Predicting the speed of sound in magmas

Several relationships have been proposed to estimate the speed of sound in two-phase suspensions (e.g. Kuster & Toksöz 1974; Kieffer 1977; Berryman 1980; Harker & Temple 1988; Commander & Prosperetti 1989; Atkinson & Kytömaa 1992), and employed for bubbly magmas (e.g. Chouet 1996; Kumagai & Chouet 2000; Morrissey & Chouet 2001; Neuberg & O'Gorman 2002; Karlstrom & Dunham 2016). To compare all these models with the results of eq. (35) based on the coupled phase theory, we considered a suspension of bubbles of an ideal gas suspended in water (see Table 3 for thermodynamic properties of the phases). Fig. 8(a) displays the comparison of the speed of sound estimated with the different models for $10^{-3} \leq f \leq 10^3$ Hz. The models neglecting the evolution of the temperature of the phases (Kuster & Toksöz 1974; Berryman 1980; Harker & Temple 1988; Atkinson & Kytömaa 1992; Neuberg & O'Gorman 2002; Karlstrom & Dunham 2016) give the same results as eq. (42), underestimating the speed of sound and do not capturing its dispersion. When a material is compressed or decompressed, the temperature of its constituents changes accordingly, inducing their thermal expansions, which oppose the change of volume resulting from the change in pressure. Consequently, neglecting the thermal effects results in overestimating the ratio ($d\rho*/dP$), and in turn, underestimating compressional waves velocity. In magmas and at low frequency, the difference between the isothermal and isentropic speed of sounds is, however, small when a gas phase is present (Fig. 7). Neglecting the evolution of the temperature of the phases is thus an acceptable assumption for bubbly magmas at low frequencies ($f < \sim 1$ Hz in Fig. 4) given the uncertainty on the thermodynamic properties of the constituents. At higher frequencies, the isothermal assumption results in a large underestimation of the P-wave velocity in a bubbly magma (of $\sim$200 m s^{-1} in andesite with $\phi_g \approx 0.10$; Fig 7f). On the contrary, in the absence of exsolved volatiles, the isothermal assumption results in a significant underestimation of the speed of sound ($\sim$50 m s^{-1} in Fig. 6f) compared with the isentropic case at any frequency.

Other relationships account for the thermal effects during the propagation of an acoustic wave. The model proposed by Kieffer (1977) predicts P-wave velocity between the upper and lower bounds but does not capture the dispersion of the sound (Fig. 8a). In this model, while the temperature changes are accounted for in the gas phase, they are neglected in the liquid. As a result, the compression and decompression are isentropic in the gas and isothermal in the liquid, which explains why this model predicts speed of sounds between those predicted with eqs (42) and (45). The lack of sound dispersion results from the absence of heat exchange between the phases in this model.

The relationship proposed by Commander & Prosperetti (1989) and employed by Chouet (1996), Kumagai & Chouet (2000) and Morrissey & Chouet (2001) accounts for the exchange of heat from the bubbles to the liquid and captures the increase of the speed of sound at approximatively the same range of frequencies as eq. (35) (Fig. 8a). The evolution of the temperature in the liquid is, however, neglected in this model. Consequently, it predicts sound speeds slower than eq. (35) for all frequencies $< 10^3$ Hz. This model also considers the dynamics of the interface between the gas bubbles and surrounding liquid, a phenomenon not accounted for in our model. The dynamics of the bubbles are expected to cause a sudden increase in sound speed at a resonance frequency, which depends on the bubble radius (Commander & Prosperetti 1989; Chouet 1996) and which is not captured in eq. (35) (Fig. 8b). In magmas, the resonance frequency of bubbles is on the order of the kHz (Chouet 1996). This is above the frequencies usually used in geophysics and can be ignored for most applications.

It should be noted that another increase in the speed of sound is expected for each discrete phase at higher frequencies than explored herein (Temkin 2000). These velocity jumps result from the translational relative motions between the liquid and the discrete phases. As for heat, the constituents of the suspension exchange momentum during the propagation of an acoustic perturbation because of their relative motions. The rates of momentum transfer in the suspension depend on the coefficients of momentum exchange given by eqs (24) and (25). The evolution of the relative velocity between the carrier and suspended phases is (here between the liquid and the gas):

$$\partial_t\,(u-w) + \nu_{lg}\,(u-w) \;=\; 0 \tag{53}$$

where ν_{lg} is the critical frequency above which translational effect cannot be neglected. It is defined as the inverse of the characteristic time needed for the relative velocity between the gas and liquid phases to vanish:

$$\nu_{lg} = \beta_{lg}\left(\frac{1}{\phi_l \rho_l} + \frac{1}{\phi_g \rho_g}\right) \tag{54}$$

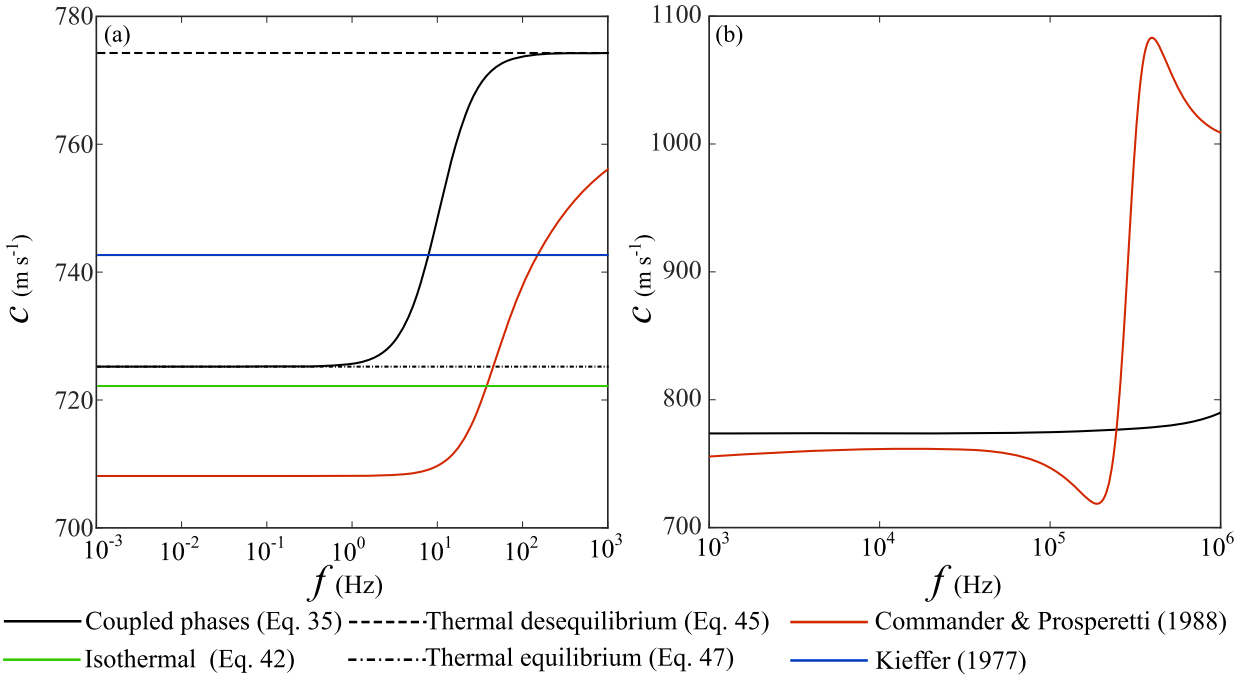

Figure 8. (a) Comparison of sound speeds predicted by various model in a suspension of gas bubbles in water for $10^{-3} \leq f \leq 10^{3}$ Hz. (b) Comparison of the speed of sound computed with eq. (35) and with eq. (41) in Commander & Prosperetti (1989) for $10^{3} \leq f \leq 10^{6}$. The properties of the fluid are the same as in (a). The density of the water and gas were calculated following eqs (8) and (9) in Kieffer (1977). The bulk modulus and coefficient of thermal expansion, $K_g = P$, $\alpha_g = 1/T$. The heat capacity of the gas is calculated as $C_{Pg} = (\gamma/(\gamma-1))R/M_g$, where γ is the heat capacity ratio ($\gamma = 1.4$), R is the ideal gas constant and M_g is the molar mass of the gas.

Similarly, the critical frequency for translational relative motion between the solids and liquid, ν_{ls}, is:

$$\nu_{lg} = \beta_{ls}\left(\frac{1}{\phi_l \rho_l} + \frac{1}{\phi_s \rho_s}\right) \tag{55}$$

When $f > \max(\nu_{ls},\nu_{lg})$ the magnitude of the relative velocity between the carrier liquid and discrete phases becomes significant and cannot be ignored when computing the speed of sound in the suspension. At these frequencies, the assumption of homogeneity required to express eq. (36) is violated such that eq. (45) cannot be employed to estimate the velocity of compressional waves. The relative motions between the phases cause the increase in the speed of sound predicted by eq. (35) observed in Fig. 8(b). The critical frequency for translational effects is inversely proportional to the dynamic viscosity of the liquid phases. For magmas, ν_{lg} and ν_{ls} are far above (>1 MHz) the maximum frequencies considered here. The influence of the translational relative motions on the speed of sound can thus be safely neglected in magmas for most geophysical applications.

4.2 Limit of validity of the model

In a suspension, the initiation of interactions between the discrete solid particles marks the onset of rigidity and the transition from liquid- to solid-like elastic body. In our model, while contacts are neglected, we accounted for the exchange of momentum between neighbouring crystals through lubrication forces. The initiation of lubricated interactions between neighbouring particles has been suggested to result in an increase in the speed of sound, marking the onset of rigidity in the suspensions (Esquivel-Sirvent *et al*. 1995). The experiment from these authors was performed at frequencies of the order of MHz, which are far above those considered in our model. Equation (21) shows that for identical solid volume fraction, I_{ss} varies as a function of $\eta k^2/\rho_s$. For magmas and perturbations in the range of frequency used in geophysics, $\sim 10^{-9} < \eta k^2/\rho_s < \sim 10^{1}$, so that the influence of lubrication on the speed of sound is negligible (Fig. 6b). As a result, the sharp increase of the velocity of the compressional waves and the emergence of shear waves (Caricchi *et al*. 2008) caused by the initiation of contact between the crystals have negligible precursory velocity increase due to lubrication.

Since the influence of the contact between the solids is beyond the scope of our model, the initiation of a fragile contact network (Bergantz *et al*. 2017) between the crystals at magma/mush transition represents the limit of its applicability. We can nevertheless qualify how the transition to rigidity may occur. The volume fraction at which a continuous contact network forms (at random loose packing) in a magma depends on the sizes, shapes, orientations and roughnesses of the crystals. It can be significantly larger than $\phi_l \approx 0.36$, the minimum random close packing calculated for frictionless and monodisperse spheres (Bergantz *et al*. 2017). The difference between random loose and close packings is expressed in the coordination numbers (average number of particle–particle contacts per particle), which is larger at random close packing than at random loose packing. The transition between the two packings occurs as a consequence of the reorganization of the crystal network due to contact sliding and particle non-affine motions. The increase in the coordination number raises the rigidity of the suspension and the speed of sound. Thus, the rigidity modulus is expected to increase progressively with the decreases of ϕ_f between the random loose and close packings. Contacts between solids are implicitly accounted for in the effective medium theory (e.g. Kuster & Toksöz

1974; Berryman 1980) and the Hertz–Mindlin contact theory. In dense suspensions where solids are in cohesionless contact, the bulk and rigidity moduli also depend on the confining pressure and amplitude of the perturbation, which affects the non-affine motions of the crystals, contact slidings and shear dilatancy (e.g. Makse *et al*. 2004; Brum *et al*. 2019). Such phenomena may induce either strengthening or weakening of the rigidity of the suspension because of the changes in the contact network (Van den Wildenberg *et al*. 2013). The effective medium theory is not able to account for the relaxations associated with changes in the contact network and usually overestimates the shear modulus (Makse *et al*. 2004). As a result, the applicability of methods based on the effective medium theory to compute the speed of sound between the random loose and random close packing is uncertain given the proneness of the crystal network to structural reordering and non-affine motions.

In addition to the absence of contact between particles, we made assumptions when deriving the conservation equations that may affect the calculated sound speed. We neglected the mass transfers associated with the precipitation or melting of crystals and the growth, dissolution or nucleation of gas bubbles. The importance of the mass transfers on the acoustic properties of a suspension depends on the rates of mass exchange between the constituents (Fuster & Montel 2015). In magmas, the exsolution or dissolution of the volatiles depends on the changes in their solubility in the melt phase, which is mainly controlled by the pressure changes. The nucleation of bubbles is expected to occur during a short period (Toramaru 1995) and requires a large supersaturation pressure ($>$ 5 MPa) even in the presence of crystals (Hurwitz & Navon 1994; Shea 2017). In our model, we considered small perturbations and the magma being initially at thermodynamic equilibrium (no steady mass or heat transfers). Thereby, the small amplitudes of the perturbations in pressure are not expected to trigger the nucleation of bubbles, which requires large amplitude waves (Rothery *et al*. 2007). The rate of the exchange of mass between the dissolved and exsolved volatiles is controlled by the bubbles sizes and the diffusion coefficient of the volatiles species in the melt phase (Toramaru 1995). The competition between diffusion and the rate of pressure change can be measured by the ratio of the diffusive timescale over the decompression timescale (Lensky *et al*. 2004). The diffusivity coefficient of water (the most common volatile in magma) is low (between $\sim 10^{-13}$ and $\sim 10^{-10}$ m^2 s^{-1}; Zhang & Behrens 2000) so that mass transfer between the melt and gas phases is negligible (i.e. the diffusive ratio is $>$ 1) when changes in pressure are faster than $\sim 10^{-2}$–10^{-4} Hz for bubbles of 10–100 μm in radius, respectively. Similarly, the rates of the precipitation or melting of the crystals in magmas are small (e.g. $\sim 10^{-13}$ and 10^{-12} m s^{-1} for crystal growth; Hawkesworth *et al*. 2004) so that we do not expect the mass transfer between the liquid and solid phases to have a significant influence on the velocity of a compressional wave in magma.

Heat and mass exchanges between the phases are controlled by the coupling terms (β_{ls}, β_{lg}, γ_{ls} and γ_{lg}), which are based on empirical correlations. The choice for the correlations employed to calculate the coefficients of momentum exchange, β_{ls} and β_{lg}, influences the two critical frequencies, ν_{ls} and ν_{lg}, at which the translational relative velocities between the suspended and carrier phases start to significantly influence sound speed (when $f > 10^5$ Hz in Fig. 8b). Here, we considered the creeping and steady flow of the liquid around the discrete phases because of the dynamic viscosity of the melt allowing us to neglect inertial and unsteady terms. We employed a Stokes law for high porosity ($\phi_l > \sim 0.893$) as usually used in the coupled phase theory (e.g. Harker & Temple 1988; Atkinson & Kytömaa 1992; Evans & Attenborough 1997). For lower porosity ($\phi_l < \sim 0.893$), we used a Kozeny–Carman relationship instead of the Stokes law to account for the influence of the presence of the surrounding crystals and the associated decrease in permeability. The maximum difference between the momentum exchanges coefficients predicted by the Stokes and Kozeny–Carman relationships occurs at the maximum packing fraction and reaches $\sim$1 order of magnitude. Therefore, account for the Stokes law instead of the Kozeny–Carman law would result in a decrease of the critical frequencies, β_{ls} and β_{lg}, of $\sim$1 order of magnitude at maximum. The two critical frequencies, β_{ls} and β_{lg}, calculated considering a Stokes law remain above the range of frequency considered (10^{-3}–10^3 Hz). As a result, in the range of the frequency considered here, the choice of the law for the exchange of momentum has a negligible influence on the calculated speed of sound in magma.

Similarly, the choice of the empirical relationship employed to predict Nusselt number in the coefficient of heat transfer between the phases, γ_{ls} and γ_{lg}, impacts the critical frequencies at which the transition between thermal equilibrium and disequilibrium regimes occurs. We used the correlation proposed by Gunn (1978) to obtain an expression depending on the porosity of the suspension. This expression also accounts for the influence of the relative velocity between the carrier and suspended phases. We showed that within the range of frequency considered, the relative velocity between the constituents is negligible. As a result, the influence of the relative motion between the constituents on the rates of heat exchange is weak and can be neglected. Furthermore, other empirical relationships predicting the Nusselt number exist (e.g. Ranz 1952; Li & Mason 2000) but often reduce to $Nu = 2$ in the absence of relative flow between the constituents, which is the same Nu as predicted by eq. (31) when $\phi_l = 1$. At the minimum porosity ($\phi_l = 0.36$), eq. (31) predicts $Nu = \sim 4$. As a result, employing another empirical correlation to calculate the Nusselt number will tend to decrease the two critical frequencies, ${\tau_g}^{-1}$ and ${\tau_g}^{-1}$, by a factor of 2 at maximum. The two theoretical maximum and minimum wave velocities (eqs 45 and 47) remain unchanged since the correlation of the Nusselt number only affects the rate of the heat exchanges but not the equilibrium temperature predicted by eq. (46).

4.3 Implication in volcanology

Our results have implications for the interpretation of seismic signals recorded around volcanoes. Long period (LP) events are thought to result from the acoustic excitation of cracks (e.g. Chouet 1986; Kumagai & Chouet 2000) or in the volcanic conduits filled with fluid (magmas, water, gas, etc., e.g. Jousset *et al*. 2003, 2004) with the surrounding solid rock. The velocity of compression waves in the magma located in the cracks or conduit affects the resonance frequency, radiation attenuation. Our model shows that compressional waves propagate faster at high frequency ($>$100 Hz) than at low frequency ($<$ 1 Hz) when the magma contains exsolved volatiles. Consequently, the resonance frequency of a crack filled with bubbly magma will be higher (and the radiation attenuation lower) at a high frequency than at a low one. This effect accentuates the dispersive behavior of the crack and tube waves that propagate in volcanic cavities (Chouet 1986; Ferrazzini & Aki 1987).

The detection of exsolved volatiles and estimation of their volume fraction in magma is important to assess volcanic hazards. Tomography images of seismic waves velocity are an interesting tool to map compositional changes in magma reservoirs. Our model provides a way to assess how the speed of sound in magma depends on both

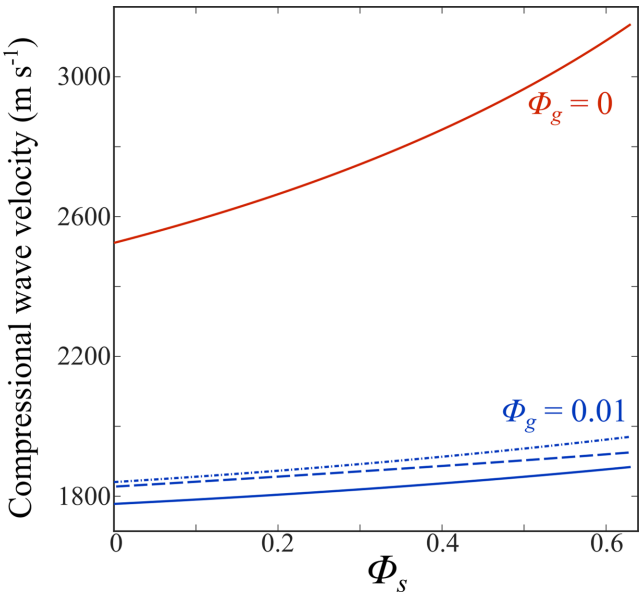

Figure 9. Evolution of the compressional wave velocity as a function of the solid volume fraction. The red and blue curves were computed with $\phi_g = 0$ and 0.01, respectively. The solid curves, dashed and dotted–dashed curves correspond to frequencies of 1, 10 and 100 Hz, respectively (when $\phi_g = 0$, the three curves collapse because of the vertical resolution). The material properties of the constituents are indicated in Table 2.

the crystal and the exsolved volatiles contents. Crystals increase the velocity of compressional waves but weakly affect the dispersion of sound in the magma (Fig. 9). The presence of gas bubble greatly decreases compressional wave velocity and induces the dispersion of sound. The difference between the speed of sound at high and low frequencies is proportional to the gas volume fraction (Fig. 7). Consequently, the comparison of tomography images computed for different frequencies at low and high frequencies might help in highlighting the presence of gas when mapping magma reservoirs.

5 CONCLUSION

We developed an analytical model to estimate the speed of sound in magmas consisting of a suspension of solids and/or gas bubbles in a viscous liquid. Our model shows that the velocity of compressional waves in a magma varies nonlinearly with frequency between two asymptotic bounds. The nonlinearity is caused by two successive speed increases as frequency increases caused by increasing levels of thermal disequilibrium between the phases. These two bounds correspond to the speed of sound when all the constituents of the magma are in thermal equilibrium (lower bound) and when the heat exchanges between the phases are neglected (upper bound). Our results show that below 10^3 Hz, lubrication forces have a negligible influence on the speed of sound ($\delta v < 10^{-4}$ m s^{-1}). We simulated the cooling of three magmas representative of the diversity of compositions commonly encountered in arc magmatism and applied our model to calculate corresponding the speed of sound. Results show that the presence of gas in a magma yields a sharp decrease in the velocity of sound and enhances significantly its dispersion. The existence of crystals in a magma increase *P*-wave velocity but does not affect significantly its dispersion. We found that the exchanges of heat between the constituents may be neglected in crystal-bearing magmas, but that they cannot be ignored once a gas phase is present. Finally, we compared the speed of sound in a water–gas mixture that is predicted by our model to those given by other relationships usually used by authors for magmas or water in the range 10^{-3}–10^3 Hz. The difference between our model of the velocity of compressional waves and literature values results from the simplifications and assumptions made when considering the evolution of the temperature of the phases and the heat exchanges. In water, these differences typically range from 0.5 to 8 per cent and are largest at frequencies > 10 Hz.

DATA AVAILABILITY

All the data and code related to this manuscript are available in the supplementary materials (online).

ACKNOWLEDGEMENTS

AC was supported by the National Science Foundation grant EAR-1950113 and doctoral research allocation by the french Ministère de l'Enseignement Supérieur et de la Recherche et de l'innovation. CA was supported by the European Union's Horizon 2020 research and innovation programme under the Marie Sklodowska-Curie grant agreement no. 794594. GWB was supported by National Science Foundation grants DGE-1256068, EAR-1447266 and EAR-1950113. AB was supported by Agence Nationale pour la Recherche grant ANR-19-CE31-0007. The authors thank Juan Carlos Afonso and an anonymous reviewer for their reviews that improved this manuscript and Lapo Boschi for his editorial handling.

REFERENCES

Annen, C., Blundy, J.D., Leuthold, J. & Sparks, R.S.J., 2015. Construction and evolution of igneous bodies: towards an integrated perspective of crustal magmatism, *Lithos,* **230,** 206–221.

Atkinson, C.M. & Kytömaa, H.K., 1992. Acoustic wave speed and attenuation in suspensions, *Int. J. Multiphase Flow,* **18,** 577–592, Elsevier.

Bachmann, O. & Bergantz, G.W., 2004. On the origin of crystal-poor rhyolites: extracted from batholithic crystal mushes, *J. Petrol.,* **45,** 1565–1582, Oxford University Press.

Bachmann, O. & Huber, C., 2019. The inner workings of crustal distillation columns; the physical mechanisms and rates controlling phase separation in silicic magma reservoirs, *J. Petrol.,* **60,** 3–18, Oxford University Press.

Benyahia, S., Syamlal, M. & O'Brien, T.J., 2006. Extension of Hill–Koch–Ladd drag correlation over all ranges of Reynolds number and solids volume fraction, *Powder Technol.,* **162,** 166–174, Elsevier.

Bergantz, G.W., Schleicher, J.M. & Burgisser, A., 2017. On the kinematics and dynamics of crystal-rich systems, *J. geophys. Res.: Solid Earth,* **122,** 6131–6159.

Berryman, J.G., 1980. Long-wavelength propagation in composite elastic media I. Spherical inclusions, *J. acoust. Soc. Am.,* **68,** 1809–1819, Acoustical Society of America.

Brennen, C.E., 2005. *Fundamentals of Multiphase Flow,* Cambridge University Press.

Brum, J., Gennisson, J.L., Fink, M., Tourin, A. & Jia, X., 2019. Drastic slowdown of the Rayleigh-like wave in unjammed granular suspensions, *Phys. Rev. E,* **99,** 042902, APS.

Carcione, J.M., Farina, B., Poletto, F., Qadrouh, A.N. & Cheng, W., 2020. Seismic attenuation in partially molten rocks, *Phys. Earth planet. Inter.,* **309,** 106568.

Caricchi, L., Annen, C., Blundy, J., Simpson, G. & Pinel, V., 2014. Frequency and magnitude of volcanic eruptions controlled by magma injection and buoyancy, *Nat. Geosci.,* **7,** 126–130, Nature Publishing Group.

Caricchi, L., Burlini, L. & Ulmer, P., 2008. Propagation of P and S-waves in magmas with different crystal contents: insights into the crystallinity of magmatic reservoirs, *J. Volc. Geotherm. Res.,* **178,** 740–750, Elsevier.

Caricchi, L., Burlini, L., Ulmer, P., Gerya, T., Vassalli, M. & Papale, P., 2007. Non-Newtonian rheology of crystal-bearing magmas and implications for magma ascent dynamics, *Earth planet. Sci. Lett.,* **264,** 402–419, Elsevier.

Carrara, A., Burgisser, A. & Bergantz, G.W., 2019. Lubrication effects on magmatic mush dynamics, *J. Volc. Geotherm. Res.,* **380,** 19–30, Elsevier.

Carrara, A., Burgisser, A. & Bergantz, G.W., 2020. The architecture of intrusions in magmatic mush, *Earth planet. Sci. Lett.,* **549,** 116539.

Cassidy, M., Manga, M., Cashman, K. & Bachmann, O., 2018. Controls on explosive-effusive volcanic eruption styles, *Nat. Commun.,* **9,** 1–16, Nature Publishing Group.

Chouet, B., 1986. Dynamics of a fluid-driven crack in three dimensions by the finite difference method, *J. geophys. Res.: Solid Earth,* **91,** 13967–13992.

Chouet, B.A., 1996. New Methods and Future Trends in Seismological Volcano Monitoring, in *Monitoring and Mitigation of Volcano Hazards*eds. Scarpa, R. & Tilling, R.I., pp. 23–97, Berlin, Heidelberg: Springer. doi:10.1007/978-3-642-80087-0_2.

Collier, L., Neuberg, J.W., Lensky, N., Lyakhovsky, V. & Navon, O., 2006. Attenuation in gas-charged magma, *J. Volc. Geotherm. Res.,* **153,** 21–36, Elsevier.

Commander, K.W. & Prosperetti, A., 1989. Linear pressure waves in bubbly liquids: comparison between theory and experiments, *J. acoust. Soc. Am.,* **85,** 732–746, Acoustical Society of America.

De Siena, L., Thomas, C., Waite, G.P., Moran, S.C. & Klemme, S., 2014. Attenuation and scattering tomography of the deep plumbing system of Mount St. Helens, *J. geophys. Res.: Solid Earth,* **119,** 8223–8238, Wiley Online Library.

Degruyter, W., Parmigiani, A., Huber, C. & Bachmann, O., 2019. How do volatiles escape their shallow magmatic hearth?, *Philos. Trans. R. Soc. A,* **377,** 20180017, The Royal Society Publishing.

Delph, J.R., Ward, K.M., Zandt, G., Ducea, M.N. & Beck, S.L., 2017. Imaging a magma plumbing system from MASH zone to magma reservoir, *Earth planet. Sci. Lett.,* **457,** 313–324.

Dingwell, D.B. & Webb, S.L., 1989. Structural relaxation in silicate melts and non-Newtonian melt rheology in geologic processes, *Phys. Chem. Miner.,* **16,** 508–516, Springer.

Duan, X., 2014. A general model for predicting the solubility behavior of H2O–CO2 fluids in silicate melts over a wide range of pressure, temperature and compositions, *Geochim. Cosmochim. Acta.,* **125,** 582–609.

Dufek, J. & Bachmann, O., 2010. Quantum magmatism: magmatic compositional gaps generated by melt-crystal dynamics, *Geology,* **38,** 687–690, Geological Society of America.

Eichelberger, J. & Izbekov, P., 2000. Eruption of andesite triggered by dyke injection: contrasting cases at Karymsky Volcano, Kamchatka and Mt Katmai, Alaska, *Philos. Trans. R. Soc. Lond. Ser. A: Math. Phys. Eng. Sci.,* **358,** 1465–1485.

Ergun, S., 1952. Fluid flow through packed columns, *Chem. Eng. Prog.,* **48,** 89–94.

Esquivel-Sirvent, R., Green, D.H. & Yun, S.S., 1995. Critical mechanical behavior in the fluid/solid transition of suspensions, *Appl. Phys. Lett.,* **67,** 3087–3089, American Institute of Physics.

Evans, J.M. & Attenborough, K., 1997. Coupled phase theory for sound propagation in emulsions, *J. acoust. Soc. Am.,* **102,** 278–282, Acoustical Society of America.

Ferrazzini, V. & Aki, K.,,1987. Slow waves trapped in a fluid-filled infinite crack: implications for volcanic tremor,. *J. geophys. Res.: Solid Earth,* **92,** 9215–9223, Wiley Online Library.

Fuster, D. & Montel, F., 2015. Mass transfer effects on linear wave propagation in diluted bubbly liquids, *J. Fluid Mech.,* **779,** 598–621, Cambridge University Press.

Ghiorso, M.S., 2004. An equation of state for silicate melts. I. Formulation of a general model, *Am. J. Sci.,* **304,** 637–678, American Journal of Science.

Gidaspow, D., 1994. *Multiphase Flow and Fluidization: Continuum and Kinetic Theory Descriptions,* Academic Press.

Gumerov, N.A., Ivandaev, A.I. & Nigmatulin, R.I., 1988. Sound waves in monodisperse gas-particle or vapour-droplet mixtures, *J. Fluid Mech.,* **193,** 53–74, Cambridge University Press.

Gunn, D.J., 1978. Transfer of heat or mass to particles in fixed and fluidised beds, *Int. J. Heat Mass Transfer,* **21,** 467–476, Elsevier.

Hammond, W.C. & Humphreys, E.D., 2000. Upper mantle seismic wave attenuation: effects of realistic partial melt distribution, *J. geophys. Res.: Solid Earth,* **105,** 10987–10999, Wiley Online Library.

Harker, A.H. & Temple, J.A.G., 1988. Velocity and attenuation of ultrasound in suspensions of particles in fluids, *J. Phys. D Appl. Phys.,* **21,** 1576, IOP Publishing.

Hawkesworth, C., George, R., Turner, S. & Zellmer, G., 2004. Time scales of magmatic processes, *Earth planet. Sci. Lett.,* **218,** 1–16.

Hier-Majumder, S., 2008. Influence of contiguity on seismic velocities of partially molten aggregates, *J. geophys. Res.: Solid Earth,* **113,** Wiley Online Library.

Holness, M.B., 2018. Melt segregation from silicic crystal mushes: a critical appraisal of possible mechanisms and their microstructural record, *Contrib. Mineral. Petrol.,* **173,** 48, Springer.

Hooft, E.E.E. *et al.*, 2019. Seismic imaging of Santorini: subsurface constraints on caldera collapse and present-day magma recharge, *Earth planet. Sci. Lett.,* **514,** 48–61.

Huang, H.-H., Lin, F.-C., Schmandt, B., Farrell, J., Smith, R.B. & Tsai, V.C., 2015. The Yellowstone magmatic system from the mantle plume to the upper crust, *Science,* **348,** 773–776, American Association for the Advancement of Science.

Huber, C., Bachmann, O. & Dufek, J., 2011. Thermo-mechanical reactivation of locked crystal mushes: melting-induced internal fracturing and assimilation processes in magmas, *Earth planet. Sci. Lett.,* **304,** 443–454.

Hurwitz, S. & Navon, O., 1994. Bubble nucleation in rhyolitic melts: experiments at high pressure, temperature, and water content, *Earth planet. Sci. Lett.,* **122,** 267–280, Elsevier.

Jousset, P., Neuberg, J. & Jolly, A., 2004. Modelling low-frequency volcanic earthquakes in a viscoelastic medium with topography, *Geophys. J. Int.,* **159,** 776–802.

Jousset, P., Neuberg, J. & Sturton, S., 2003. Modelling the time-dependent frequency content of low-frequency volcanic earthquakes, *J. Volc. Geotherm. Res.* **128,** 201–223.

Karlstrom, L. & Dunham, E.M., 2016. Excitation and resonance of acoustic-gravity waves in a column of stratified, bubbly magma, *J. Fluid Mech.,* **797,** 431–470, Cambridge University Press.

Karlstrom, L., Rudolph, M.L. & Manga, M., 2012. Caldera size modulated by the yield stress within a crystal-rich magma reservoir, *Nat. Geosci.,* **5,** 402–405, Nature Publishing Group.

Kieffer, S.W., 1977. Sound speed in liquid-gas mixtures: water-air and water-steam, *J. geophys. Res.,* **82,** 2895–2904, Wiley Online Library.

Kiser, E., Levander, A., Zelt, C., Schmandt, B. & Hansen, S., 2018. Focusing of melt near the top of the Mount St. Helens (USA) magma reservoir and its relationship to major volcanic eruptions, *Geology,* **46,** 775–778, GeoScienceWorld.

Kumagai, H. & Chouet, B.A., 2000. Acoustic properties of a crack containing magmatic or hydrothermal fluids, *J. geophys. Res.: Solid Earth,* **105,** 25493–25512, Wiley Online Library.

Kuster, G.T. & Toksöz, M.N., 1974. Velocity and attenuation of seismic waves in two-phase media: Part I. Theoretical formulations, *Geophysics,* **39,** 587–606, Society of Exploration Geophysicists.

Kytömaa, H.K., 1995. Theory of sound propagation in suspensions: a guide to particle size and concentration characterization, *Powder Technol.,* **82,** 115–121, Elsevier.

Lensky, N.G., Navon, O. & Lyakhovsky, V., 2004. Bubble growth during decompression of magma: experimental and theoretical investigation, *J. Volc. Geotherm. Res.,* **129,** 7–22, Elsevier.

Li, J. & Mason, D.J., 2000. A computational investigation of transient heat transfer in pneumatic transport of granular particles, *Powder Technol.,* **112,** 273–282, Elsevier.

Mader, H.M., Llewellin, E.W. & Mueller, S.P., 2013. The rheology of two-phase magmas: a review and analysis, *J. Volc. Geotherm. Res.,* **257,** 135–158, Elsevier.

Makse, H.A., Gland, N., Johnson, D.L. & Schwartz, L., 2004. Granular packings: nonlinear elasticity, sound propagation, and collective relaxation dynamics, *Phys. Rev. E,* **70,** 061302, APS.

Margulies, T.S. & Schwarz, W.H., 1994. A multiphase continuum theory for sound wave propagation through dilute suspensions of particles, *J. acoust. Soc. Am.,* **96,** 319–331, Acoustical Society of America.

Martel, C., Pichavant, M., Holtz, F., Scaillet, B., Bourdier, J.-L. & Traineau, H., 1999. Effects of f O2 and H2O on andesite phase relations between 2 and 4 kbar, *J. geophys. Res.: Solid Earth,* **104,** 29453–29470, Wiley Online Library.

Marzougui, D., Chareyre, B. & Chauchat, J., 2015. Microscopic origins of shear stress in dense fluid–grain mixtures, *Granular Matter,* **17,** 297–309, Springer.

Mavko, G.M., 1980. Velocity and attenuation in partially molten rocks, *J. geophys. Res.: Solid Earth,* **85,** 5173–5189, Wiley Online Library.

Morrissey, M.M. & Chouet, B.A., 2001. Trends in long-period seismicity related to magmatic fluid compositions, *J. Volc. Geotherm. Res.,* **108,** 265–281.

Neuberg, J. & O'Gorman, C., 2002. A model of the seismic wavefield in gas-charged magma: application to Soufrière Hills Volcano, Montserrat, *Geol. Soc., Lond. Mem.,* **21,** 603–609, Geological Society of London.

Pallister, J.S., Hoblitt, R.P., Meeker, G.P., Knight, R.J. & Siems, D.F., 1996. Magma mixing at Mount Pinatubo: petrographic and chemical evidence from the 1991 deposits, *Fire and Mud: Eruptions and Lahars of Mount Pinatubo, Philippines,* pp. 687–731, PHIVOLCS and University of Washington, Seattle.

Parmigiani, A., Faroughi, S., Huber, C., Bachmann, O. & Su, Y., 2016. Bubble accumulation and its role in the evolution of magma reservoirs in the upper crust, *Nature,* **532,** 492–495, Nature Publishing Group.

Paulatto, M., Annen, C., Henstock, T.J., Kiddle, E., Minshull, T.A., Sparks, R.S.J. & Voight, B., 2012. Magma chamber properties from integrated seismic tomography and thermal modeling at Montserrat, *Geochem. Geophys. Geosyst.,* **13,** Wiley Online Library.

Petford, N., 2009. Which effective viscosity?, *Mineral. Mag.,* **73,** 167–191, GeoScienceWorld.

Ranz, W.E., 1952. Evaporation from drops, Parts I & II, *Chem. Eng. Prog.*, **48,** 141–146.

Rothery, D.A., Sumner, J.M., Spieler, O. & Dingwell, D.B., 2007. Impact vesiculation? a new trigger for volcanic bubble growth and degassing, *Earth Discuss.,* **2,** 151–167.

Shea, T., 2017. Bubble nucleation in magmas: a dominantly heterogeneous process?, *J. Volc. Geotherm. Res.,* **343,** 155–170, Elsevier.

Syamlal, M., Rogers, W. & OBrien, T.J., 1993. MFIX documentation theory guide, USDOE Morgantown Energy Technology Center, WV (United States).

Takahashi, R. & Nakagawa, M., 2013. Formation of a compositionally reverse zoned magma chamber: petrology of the ad 1640 and 1694 eruptions of Hokkaido-Komagatake volcano, Japan, *J. Petrol.,* **54,** 815–838, Oxford University Press.

Takei, Y., 2002. Effect of pore geometry on VP/VS: from equilibrium geometry to crack, *J. geophys. Res.: Solid Earth,* **107,** ECV 6-1-ECV 6-12, Wiley Online Library.

Temkin, S., 1998. Sound propagation in dilute suspensions of rigid particles, *J. acoust. Soc. Am.,* **103,** 838–849, Acoustical Society of America.

Temkin, S., 2000. Attenuation and dispersion of sound in dilute suspensions of spherical particles, *J. acoust. Soc. Am.,* **108,** 126–146, Acoustical Society of America.

Toramaru, A., 1995. Numerical study of nucleation and growth of bubbles in viscous magmas, *J. geophys. Res.: Solid Earth,* **100,** 1913–1931.

Valier-Brasier, T., Conoir, J.-M., Coulouvrat, F. & Thomas, J.-L., 2015. Sound propagation in dilute suspensions of spheres: analytical comparison between coupled phase model and multiple scattering theory, *J. acoust. Soc. Am.,* **138,** 2598–2612, Acoustical Society of America.

Van den Wildenberg, S., Hecke, M. van & Jia, X., 2013. Evolution of granular packings by nonlinear acoustic waves, *EPL (Europhys. Lett.),* **101,** 14004, IOP Publishing.

Waite, G.P. & Moran, S.C., 2009. VP Structure of Mount St. Helens, Washington, USA, imaged with local earthquake tomography, *J. Volc. Geotherm. Res.,* **182,** 113–122.

Wen, C.Y. & Yu, Y.H., 1966. A generalized method for predicting the minimum fluidization velocity, *AIChE J.,* **12,** 610–612, American Institute of chemical engineers New York.

Wiebe, R.A., 2016. Mafic replenishments into floored silicic magma chambers, *Am. Mineral.,* **101,** 297–310.

Zhang, Y. & Behrens, H., 2000. H2O diffusion in rhyolitic melts and glasses, *Chem. Geol.,* **169,** 243–262.

SUPPORTING INFORMATION

Supplementary data are available at *GJI* online.

compute_seismic_properties_magma.m
supplementary_material_3
supplementary_materials_1_2

Please note: Oxford University Press is not responsible for the content or functionality of any supporting materials supplied by the authors. Any queries (other than missing material) should be directed to the corresponding author for the paper.